Available online at www.sciencedirect.com
ScienceDirect
International Journal of Heat and Mass Transfer 50 (2007) 2480–2491
International Journal of HEAT and MASS TRANSFER
www.elsevier.com/locate/ijhmt

Flow and heat transfer behaviors of phase change material slurries in a horizontal circular tube

Xichun Wang [a], Jianlei Niu [a,*], Yi Li [c], Xin Wang [b], Binjiao Chen [b], Ruolang Zeng [b], Qingwen Song [c], Yinping Zhang [b]

[a] *Department of Building Service Engineering, The Hong Kong Polytechnic University, Hong Kong, PR China*
[b] *Department of Building Science, Tsinghua University, Beijing 100084, PR China*
[c] *Institute of Textiles and Clothing, The Hong Kong Polytechnic University, Hong Kong, PR China*

Received 10 July 2006; received in revised form 3 November 2006

Abstract

The flow and convective heat transfer behaviors of microencapsulated phase change material (MPCM) slurries in a horizontal circular tube have been experimentally investigated. The slurry consisted of microencapsulated 1-bromohexadecane ($C_{16}H_{33}Br$) and water, with the mass fractions of MPCM varying from 5% to 27.6%. The pressure drop and local heat transfer coefficients were measured, and the influences of capsule fractions, heating rates, and flow structures on heat transfer performance were also studied. Heat transfer coefficients measured for MPCM slurry are significantly higher than for those for single-phase fluid flow in laminar flow conditions, but exhibit more complicated phenomena at low turbulent conditions. Moreover, a new simple heat transfer correlation equation was proposed that accurately predicts the local heat transfer coefficients of laminar MPCM slurry flow in a horizontal circular tube.

Keywords: MPCM slurry; Test section; MPCM slurry; Local heat transfer coefficient; Laminar slurry flow; Turbulent slurry flow

1. Introduction

Phase change materials (PCMs) have long been used for thermal storage/control materials because of the large amount of heat absorption/release during the phase change processes, with only small temperature variations. In the last 40 years, lots of efforts have been made to enhance the energy storage capacity of structural material for solar and building applications by integrating the PCMs directly into the other materials, e.g. wallboard, concrete blocks, under floor heating system, etc. [1]. However, the thermal performances of such applications are not significant due to the low thermal conductivity of PCMs [2]. In recent years, a new approach was proposed, in which the phase change material was microencapsulated and suspended in a single-phase heat transfer fluid (e.g. as a solid–liquid suspensions) to form microencapsulated phase change material (MPCM) slurry [3]. MPCM slurries are advantageous because of latent heat effect associated with phase change process of material. The apparent specific heat capacity is much higher than conventional sensible heat effect fluid without phase change, which may greatly enhance the heat transfer performance between the fluid and heat transfer surface. In addition, the storage of MPCS during the night time for use in cooling application during the day allows for shifting and leveling the electric power load. Furthermore, the agglomeration and deposition of particles in the fluid are avoided because the core material is always separated from the carried fluid by thin plastics shell.

In previous studies, the flow and melting heat transfer characteristics of microencapsulated phase change material (MPCM) slurry at laminar flow condition have been investigated by a number of researchers. Sohn and Chen [4] observed enhanced thermal conductivity of solid–liquid slurry at a low flow velocity due to the effects of

* Corresponding author. Tel.: +852 27667781; fax: +852 27746146.
E-mail address: bejlniu@polyu.edu.hk (J. Niu).

0017-9310/$ - see front matter © 2007 Elsevier Ltd. All rights reserved.
doi:10.1016/j.ijheatmasstransfer.2006.12.024

Nomenclature

a	constant (Eq. (7)) (W m °C^2)
A	constant (Eq. (9)) (–)
c	constant (Eq. (15)) (–)
C_p	specific heat capacity
d	particle diameter (m)
D	tube diameter (m)
f	friction factor (–)
h	heat transfer coefficient (W/(m^2 °C))
ΔH	latent heat of fusion (kJ/kg)
k	thermal conductivity (W/(m °C))
L	length of test section (m)
$\dot{m}$	mass flow rate (kg/s)
Nu	Nusselt number (–)
Pr	Prandtl number (–)
ΔP	pressure drop (Pa)
q	heat flux density (W/m^2)
Q	heat rate (W)
r	radius of the test tube (m)
Re	Reynolds number (–)
T	temperature (°C)
ΔT	temperature difference (°C)
u	flow velocity (m/s)
w	mass faction (–)
x	coordinate in the axial direction (m)

Greek symbols

ρ	density (kg/m^3)
η	dynamic viscosity (Pa s)

Subscripts

1–3	melting regions of slurry in tube
c	microcapsule core
b	bulk
f	fluid
I	inlet
m	mean, melting point
o	outlet
p	particle
w	wall
wo	external wall surface
lb	based on local bulk temperature
lw	based on local wall temperature
l	liquid phase
s	solid phase
x	at axial position x

microconvection around the small solid particles. In an analytical study, Kasza and Chen [3] presented that up to a 10-fold enhancement increase of heat transfer coefficient might be obtained in some specific flow conditions, however the result has not been confirmed by the experiments. Charaunyakorn et al. [5] developed a model to predict laminar MPCS flow in a heated circular duct and showed that about 2–4 times increase in mean Nusselt number is possible in comparison with single phase fluid flow. Goel et al. [6] reported that the reduction of the rise of in-wall temperature is by up to 50% compared to a single phase flow in the same dimensionless conditions. The experimental results were compared with those predicted by the numerical simulation of Charaunyakorn et al. [5], and they found the similar trends, although the difference between them was about 45% because of supercooling of the phase change material. Other related numerical investigations of melting heat transfer of laminar flow of MPCM slurries in the circular duct include the works of Zhang and Faghri [7], Alisetti and Roy [8], Hu and Zhang [9], and Ho et al. [10].

Several past studies also attempted to deal with the flow and melting behaviors of phase change slurry in turbulent conditions. Choi et al. [11] measured the local pressure drop and heat transfer coefficient of turbulent phase change emulsion flow (mixture of water and PCM with additive of emulsion) in a horizontal tube with constant heat rates, however only the results for 10% mass particle fraction were presented. They observed a significant enhancement in heat transfer performance due to the latent heat effect when PCM was melting. They also found that both local heat transfer coefficients and pressure drop along the flow direction varied significantly when PCM was melting, which makes it difficult to apply log-mean-temperature-difference (LMTD) method to determine the heat transfer coefficient. In the case of MPCM slurry, Yamagishi et al. [12] measured the pressure drop and local convective heat transfer coefficients of turbulent microencapsulated octadecane ($C_{18}H_{38}$) slurry flow along the horizontal circular pipe with constant heating rates, and they reported that heat transfer performance of the slurry was greatly influenced by the effects of latent heat as those in the case reported by Choi et al. [11]. They also reported that such effect also depends upon the particle fractions, the degree of turbulence and heating rates on the tube wall.

The optimum design of thermal energy storage systems, which run with phase change slurry, requires a good knowledge of flow and heat transfer characteristics of two-phase slurry involved in phase change, in order to reduce the capital cost, system size, and energy consumption. Although all preliminary studies and experiments indicate promising applications of MPCM slurry as heat transfer and heat storage media, experimental investigations on MPCM slurry heat transfer characteristics appear to be limited for practical engineering design so far. This is

probably due to the particular experimental rig and narrow ranges of experimental condition for each investigation.

An experimental rig was therefore constructed at Tsinghua University to obtain reliable and sufficient data to investigate the pressure drop and heat transfer behaviors of MPCM slurry in a horizontal circular pipe when subjected to constant heating rates. The experiments covered both laminar ($Re_b < 2100$) and slightly turbulent flow ($2200 < Re_b < 4000$) with particle concentrations ranging from 5% to 27.6% by weight. The rheological behaviors for slurry at different concentrations and different temperatures were also measured.

2. Experimental approach

2.1. Microcapsule and slurry

The MPCM slurry was made of microencapsulated $C_{16}H_{33}Br$ and pure water, prepared at ITC, The Hong Kong Polytechnic University. Fig. 1 shows the optical and SEM photographs of microcapsules used in the present study. The microparticles used industrial-grade 1-bromohexadecane ($C_{16}H_{33}Br$), with a melting temperature, $T_m = 14.3$ °C, and latent heat of melting, $\Delta H_m = 160$ kJ/kg, as core material, and Amino Plastics as shell material, respectively, and the core–shell ratio was controlled to be about 7:1 by weight during the preparing process, hence the thickness of coating wall was approximately 0.3 μm. The phase transition point and latent heat of microencapsulated $C_{16}H_{33}Br$ were measured by differential scanning calorimeter (Perkin Elmer DSC7) with heating/cooling rate of 5 °C/min. The diameter of microparticle was measured by a particle characterization system (Malvern Instrument Ltd., Malvern Masterzer 2000). The volume average diameter of particles was found to be 10.112 μm. Pure water was chosen as carrier fluid because it is easy to handle and has no chemical effect on the phase change material and shell wall, and the reason is that the original form of slurry is in aqueous form and easily diluted with pure water to obtain different concentration according to various engineering applications.

2.2. Slurry properties

Flow and heat transfer characteristics are associated with the following dependant properties: density, viscosity, thermal conductivity, melting/freezing point and latent heat of fusion. These properties depend on the type of PCM, coating material, carrier fluid, the particle concentration, and the flow parameters of the slurry. Various property models have been used in the calculation of MPCM slurry system. The following sets of thermal property model applied by various researchers to the phase change slurries were used in the present study.

Densities and heat capacity of slurry are calculated by weighted fraction of the density of PCM, coating material, and water, based on the mass and energy balance [6].

$$\rho_p = \frac{8}{7}\left(\frac{d_c}{d_p}\right) \tag{1}$$

$$\rho_b = \frac{1}{w_p/\rho_p + (1 - w_p)/\rho_f} \tag{2}$$

$$C_{p,b} = w_p C_{p,p} + w_w C_{p,w} \tag{3}$$

The thermal conductivity of the microcapsule was calculated based on the composite sphere approach [13], which is given by

$$\frac{1}{k_p d_p} = \frac{1}{k_c d_c} + \frac{d_p - d_c}{k_w d_p d_c} \tag{4}$$

Although a number of models have been proposed to investigate the thermal conductivity of the solid–liquid slurry, such as those by Jeffery [14], Leak [15], and Charunyaorn et al. [5], thermal conductivity of MPCM slurry was calculated by Maxwell's relation [16] in the present analysis due to its computational simplicity.

$$k_b = k_f \frac{2k_f + k_p + 2\phi(k_p - k_f)}{2k_f + k_p - \phi(k_p - k_f)} \tag{5}$$

The properties of slurry calculated from Eqs. (1)–(5) are given in Table 1. The values of viscosity given in Table 1 were measured by a Rheometer as described in a later section.

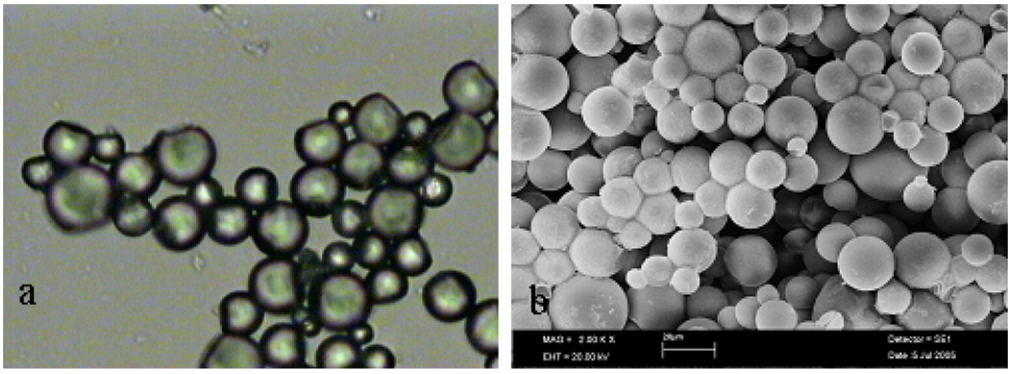

Fig. 1. (a) Optical micrograph and (b) scanning electron microscopy photograph.

Table 1
Physical properties of MPCM slurry and its components

	Density, kg m^{-3}	Specific heat, J kg^{-1} °C^{-1}	Thermal conductivity, W m^{-1} °C^{-1}	Latent heat, kJ kg^{-1}	Viscosity, mPa s at 20 °C
1-Bromohexadecae (solid) [17,18]	1006	1762	0.141	160	
1-Bromohexadecae (liquid)	998	1437	0.300		
Urea-formaldehyde [19]	1490	1675	0.433		
Water (at 20 °C) [20]	998	4183	0.599		
MPCM particle (solid)	1093	1751	0.135	140	1.00
MPCM particle (liquid)	1057	1467	0.285		
MPCM slurry (mass fraction)					
$\Phi = 0.050$	1001	4061	0.568	7.0	1.57
$\Phi = 0.100$	1004	3940	0.539	14.0	1.73
$\Phi = 0.158$	1007	3801	0.506	22.0	2.92
$\Phi = 0.204$	1010	3687	0.480	28.6	3.29
$\Phi = 0.276$	1014	3534	0.446	38.6	8.42

2.3. Experimental apparatus and method

Fig. 2 shows the schematic diagram of the experimental apparatus. The major components of the system are a slurry reservoir, two slurry pumps, a heat transfer test section, two flow meters, a differential pressure transducer, a plate heat exchanger (Tranter, Inc., Type B25), AC power supply, and a data acquisition system.

The MPCM slurry was cooled by glycol flow in a plate heat exchanger, which has heat exchanger surface of 1.76 m^2 and heat exchange capacity of 3 kW. The inlet temperature of glycol solution was maintained at −1 °C, so the temperature of MPCM slurry at the outlet of exchanger can be controlled at about 2 °C, which was much lower than the melting temperature 14.3 °C for the microencapsulated $C_{16}H_{33}Br$. Considering the supercooling degree of 10 °C of the material, such a low temperature is necessary to ensure complete solidification of all microencapsulated $C_{16}H_{33}Br$ particles in the heat exchanger.

The flow rate of slurry in the heat transfer test section was varied by manual adjustment of a mainline throttling valve and a bypass valve. The mass flow rates of fluids were determined by measuring the effluent fluid of the test section by weighting method. In normal working conditions, the slurry flow at the inlet of heat exchanger was pressurized at approximately 0.65 MPa. Both the bypass flow and main flow were fed into a slurry reservoir with a volume about 5 l. In the slurry reservoir a stirrer was installed that could keep MPCM slurry homogeneous, and the rotational speed of the stirrer can be adjusted depending on the particle fractions of the slurry.

The heat transfer test section itself was a circular stainless steel (Cri8Ni9Ti) tube, 1.46 m in length with an internal diameter of 4 mm and wall thickness of 1 mm. One of the reasons to choose such a pipe diameter is that it is the size of likely pipe diameters in HVAC applications, and another reason is to make the test rig much more compact to complete the phase change process of the

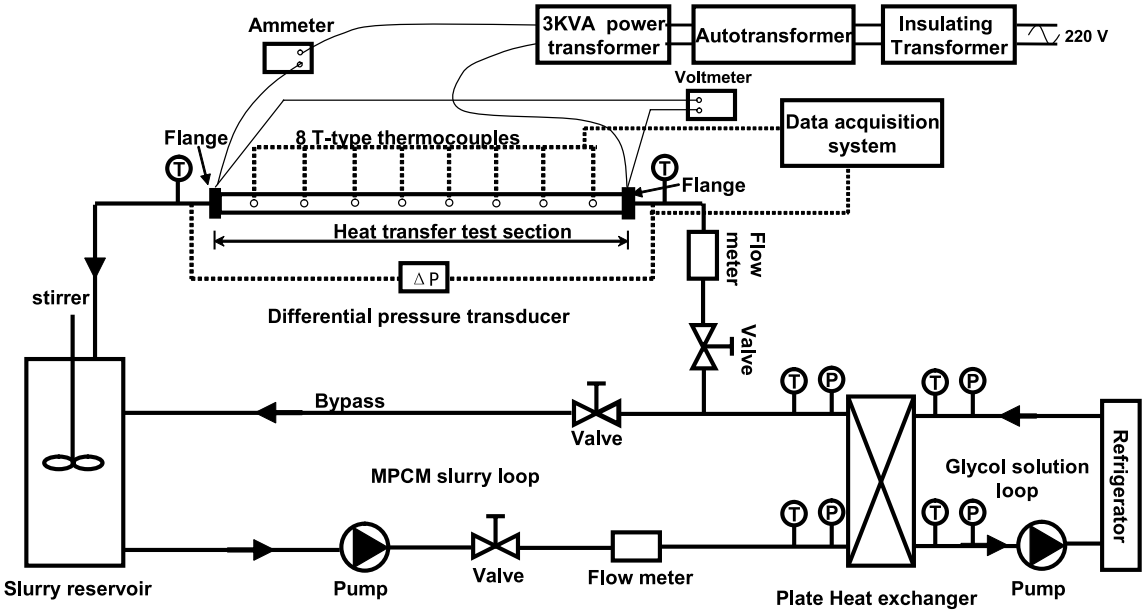

Fig. 2. Schematic diagram of experimental apparatus.

PCM particles in the test section. It has been directly connected to an AC power supply to apply a uniform heat flux. Power supply consisted of a 3 kVA power transformer, a manually controlled autotransformer, and an insulating transformer. Heating rate to the test section was controlled by the autotransformer, and the main electric loop was insulated by an insulating transformer for the safety purpose. The electrical power input was determined by measuring voltage drop across the test section and the current. Test section was fitted with flanges and isolated electrically and thermally from the adjoining entrance and existing lengths by Teflon O-rings. To minimize the heat loss to the ambient environment, the test section was thermally insulated by foam-type insulation material with a thickness of about 10 cm.

Eight T-type thermal couples were attached to the outer tube wall and the distance between the points of neighboring sensors was 0.18 m. The inlet and outlet temperatures were measured by two PT-1000 temperature sensors, which were inserted through the stainless steel tube. The temperatures of inlet and outlet of heat exchanger for each pass were also measured by inserting the T-type thermal couples into the fluid. All the temperature sensors were calibrated and measurement error was less than 0.1 °C. Pressure drop was measured across the test section using an electronic differential transducer with an accuracy of better than ±0.01 kPa. During the experiments, the variations of the temperatures at inlet and outlet of test section were controlled less than ±0.25 °C. Four pressure gages were also installed in the inlet and outlet of heat exchanger for each pass to monitor the pressure variations.

Experiments were first performed with only pure water flowing in the test section. Heat transfer runs were carried out to cover the laminar and turbulent flow conditions, and then data were compared with literature data to check the accuracy and validity of the test rig. When MPCM slurry flowed in the system, the outlet temperatures of test section were controlled at 20 °C and 25 °C, respectively to ensure all PCM particles to finish the melting process, considering PCM's melting temperature of 14.3 °C. Data points were stored at 10 min intervals. All the data from the various instruments were recorded directly to the computer through HP-34970 data acquisition system. The data used for the following analysis were made during steady state, which was indicated by the variations observed in the slurry inlet and outlet temperatures, test tube surface temperatures, pressure drop, and power input.

In this investigation, local heat transfer coefficients between the inner tube wall surface and slurry flow was defined as

$$h_x = \frac{q_{\mathrm{lw}}}{T_{\mathrm{lw}} - T_{\mathrm{lb}}} \tag{6}$$

where q_{lw} is the local heat flux at the tube wall, which was defined as the heat rate per square meters on internal tube pipe surface, T_{lw} is the local inner wall surface temperature, and T_{lb} is the local bulk mean temperature of the fluid. The local bulk mean temperature of the water can be easily calculated from the linear temperature along the test section based on the inlet and outlet temperature and tube heat flux. However, the local bulk mean temperature of the fluid accompanying phase change is not linear; therefore it cannot simply be estimated from aforementioned method. In this experiment, the local bulk mean temperatures were calculated based on the "three-region melting model" which was proposed by Choi et al. [11], although the model is quite dependent of the material property data. Table 2 shows the derived equations for the determination of the length of each region and the associated bulk mean temperature profile, $T_{\mathrm{b}}(x)$.

Table 2
Bulk temperature profile equations and length of each region

Local bulk-mean temperature		Length of the regions
Region I	$T_{\mathrm{b}}(x) = T_{\mathrm{bi}} + \frac{Q}{\dot{m}C_{\mathrm{p,s}}}\frac{x}{L}$	$\frac{L_1}{L} = \frac{\dot{m}C_{\mathrm{p,s}}(T_{\mathrm{m}} - T_{\mathrm{b,i}})}{Q}$
Region II	$T_{\mathrm{b}}(x) = T_{\mathrm{m}}$	$\frac{L_2}{L} = \frac{L - L_1 - L_3}{L}$
Region III	$T_{\mathrm{b}}(x) = T_{\mathrm{m}} + \frac{Q}{\dot{m}C_{\mathrm{p,l}}}\frac{x}{L}$	$\frac{L_3}{L} = \frac{\dot{m}C_{\mathrm{p,l}}(T_{\mathrm{b,o}} - T_{\mathrm{m}})}{Q}$

The inner wall surface temperature, T_{lw}, was derived from model of electrical and thermal conduction in the wall of the water loop test section [22], the result was given as

$$T_{\mathrm{w}} = T_{\mathrm{wo}} - C_1\frac{q_{\mathrm{w}}}{k_{\mathrm{wo}}}\left(1 + \frac{C_1}{2}\frac{aq_{\mathrm{w}}}{k_{\mathrm{wo}}^2}\right)$$

where

$$C_1 = \frac{r_{\mathrm{w}}}{r_{\mathrm{wo}}^2 - r_{\mathrm{w}}^2}\left(r_{\mathrm{wo}}^2 \ln\frac{r_{\mathrm{wo}}}{r_{\mathrm{w}}} - \frac{r_{\mathrm{wo}}^2 - r_{\mathrm{w}}^2}{2}\right) \tag{7}$$

T_{wo} and T_{i} are the tube outer and inner wall surface temperatures, respectively. r_{w} and r_{wo} are the wall inside and outside radii, respectively. k_{wo} is the thermal conductivity of the tube, $k_{\mathrm{wo}} = 14.235 + 0.013398T_{\mathrm{wo}}, a = 0.0144$, which is a constant.

Local slurry Nusselt number, Nu_{bx}, was calculated based on the local heat transfer coefficient, h_x, thermal conductivity of the slurry, k_{bx}, and the internal diameter of the test tube, D_{w}, which was defined as

$$Nu_{\mathrm{lb}} = \frac{h_x \cdot D_{\mathrm{w}}}{k_{\mathrm{lb}}} \tag{8}$$

The average heat transfer coefficient (h_{m}) and average Nusselt number (Nu_{m}), are simply calculated using arithmetic averages of local slurry heat transfer coefficients, h_x and local Nusselt numbers, Nu_{lb}, respectively.

3. Results and discussion

3.1. Rheological behaviors

The carrying fluid in MPCM slurry can generally be considered as Newtonian, as can slurry themselves if the

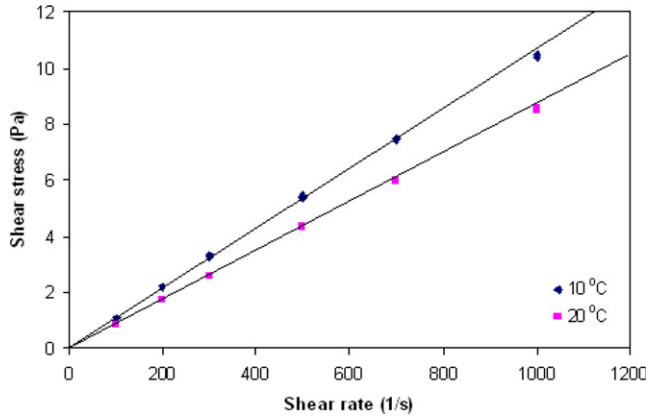

Fig. 3. Relationship of shear stress and shear rate at different temperatures for MPCS of 30 wt.%.

particle mass fraction remains low [21]. The reological behaviors of slurry with particle concentration varying from 5 to 27.6 wt.% were measured by Paar Physica MCR 300 Rheometer (Paar Scientific Ltd.), and it was found the shear stress linearly increased with shear rate and all lines were intercrossed at the original point for all above cases, therefore the slurry with concentration below 27.6 wt.% were considered to be Newtonian at the present study. As an example among them, Fig. 3 shows the relationship of shear stress and shear rate for the slurry of 27.6 wt.% at two different temperatures, at which the PCM component (core material of MPCM) was respectively at solid phase (10 °C) and liquid phase (20 °C). It is observed that the shear stress linearly increased with the shear rate in despite of the different states of PCM component they preserved, and this was attributed to the plastic shells that microencapsulate the PCM content, so that it is always the solid state spherical shape particles that are in contact with the carrying water irrespective whether the PCM content is undergoing the phase change process or not, thus the rhelogical behaviors will not be influenced by the PCM phase transition process.

In place to viscosity of the liquid, η_l, the viscosity of the slurry can be termed as apparent viscosity, η_s. Normally, the relative viscosity, which is defined as the ratio between the apparent viscosities of the slurry to that of the water, remains constant. Many different models have been proposed for the viscosity of a slurry. An empirical model predicting the solid–liquid slurry dynamic viscosity is the model of Vand [23], which was used by many previous researchers, e.g. Charunyaorn et al. [5], Mulligan et al. [24], and Goel et al. [6]. Eq. (9) can well predict the viscosity up to a particle volumetric concentration up to 37%.

$$\frac{\mu_s}{\mu_f} = \left(1 - \phi - A\phi^2\right)^{-2.5} \tag{9}$$

where ϕ is the particle volumetric fraction of the slurry. The constant, A, which quite depends on the size, the shape and the type of the particle, can be obtained experimentally. Vand [23] got the value $A = 1.16$ for the glass sphere with diameter of 0.013 cm, and Mulligan et al. [24] obtained the value $A = 3.4$ for the slurry with microencapsulated PCM particle of 10–30 μm in diameter using Eq. (9). While Yamagishi et al. [12] estimated the value $A = 3.7$ for the microencapsulated octadecane slurry with an average diameter of 6.3 μm. In the present investigation, the viscosities of microencapsulated $C_{16}H_{33}Br$ at different concentrations were measured by the Rheometer and listed in Table 1. The value $A = 4.45$ was obtained based on the viscosity data for different concentrations. Fig. 4 shows measured relative viscosities of the slurry as function of particle volumetric concentration, which fitted well by Eq. (9). The relative viscosity did not increase linearly with the particle volumetric concentrations of the slurry. The viscosity of slurry with 10% volumetric concentration is 1.2 times of that of the pure water, while the viscosity of slurry with 27% particle concentration is approximately 11 times.

The pressure drops across the test section were measured for the slurry of several particle mass concentrations when no heat flux was applied. The temperature of the slurry in the test was kept at 20 °C (near the ambient temperature), which is higher than the melting temperature of 1-bromohexadecane (T_m =14.3 °C). Pressure drop results for MPCS were expressed in term of *Darcy friction factor* [25], which was defined as

$$f = (D\Delta P/L)/\left(2\rho_b u_m^2\right) \tag{10}$$

Fig. 5 shows the relationship between the friction factor, f, and Reynolds numbers, Re_b, for slurry with three different concentrations, namely, 10%, 15.8% and 20.4%. It is observed the friction factor decreased with the increase of the Reynolds numbers as $Re_b > 2200$, which were in good accord with the predicted values calculated by using modified Blasius equation ($f = 0.12143Re^{-0.25}$), which were higher than the predicted values computed by classical Blasius equation ($f = 0.079Re^{-0.25}$) for smooth surface pipe due to the fact that the friction factor increases with the surface roughness of the tube. It appears that a transition from the laminar and turbulent flow occurred in the

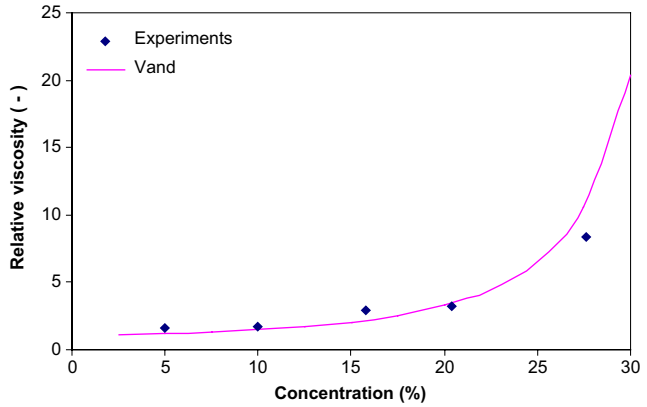

Fig. 4. Relative viscosity of slurry as a function of concentration by volume.

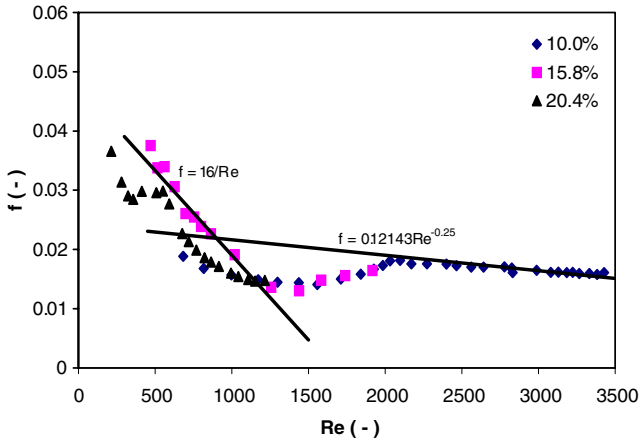

Fig. 5. Friction factor vs. Reynolds numbers for MPCM slurry at 20 °C.

Reynolds number in the range of approximately from 1200 to 2200, which is lower than the values predicted by Yamagishi et al. [12] for the MPCS with mean diameter of 6.3 μm, this is perhaps due to the particular material used in each case. In the case of laminar flow ($Re < 1200$), the friction factor decreases with increased Reynolds number. The friction factors in the laminar flow velocities fitted well with the classical model ($f = 16/Re$) based on Hagen–Poiseuille flow [25] for a circular tube only for the slurry with 15.8 wt.% particle concentration, while relatively larger discrepancy was found between the experimental values and predicted values by Hagen–Poiseuille equation for the slurries with 10.0% and 20.4% particle concentrations, and it is suspected that this might be due to the entry length effect, which is usually more significant for the laminar flow than for the turbulent flow.

3.2. Heat transfer characteristics

3.2.1. Heat transfer characteristics of pure water

The reliability and validity of the test facility were first checked by running pure water in both laminar and turbulent flow velocities, and the heat losses to the environment was evaluated from a heat balance performed on the warm water side of the test section,

$$Q_{\text{loss}} = Q_{\text{input}} - \dot{m}C_{\text{p,b}}(T_{\text{out}} - T_{\text{in}}) \tag{11}$$

where Q_{input} is the electric power imposed on the section, $\dot{m}$ and $C_{\text{p,b}}$ are the mass flow and specific heat capacity of the water, respectively, T_{in} and T_{out} are the inlet and outlet water temperatures. The heat losses to the surroundings were determined to be small (maximum 4% to the total electric power input), which was neglected in the heat transfer calculation.

Heat transfer test were also performed with only pure water flowing in the test section. The heat transfer coefficients were determined from the measured electric power input, Q_{input}, local wall temperatures, and calculated local liquid temperatures. In the case of turbulent flow, the heat transfer coefficients were compared with the predicted values calculated by using Eq. (12), which was proposed by Choi and Cho [26] for convective heat transfer of a single-phase fluid in both developing and developed flow region with a constant heat flux.

$$Nu_x = 0.00425 Re_{\text{lb}}^{0.979} Pr_{\text{lb}}^{0.4} (\mu_{\text{lw}}/\mu_{\text{lb}})^{-0.11} \tag{12}$$

where the local Reynolds number, Re_{lb}, local Prandtl number, Pr_{lb}, and dynamic viscosity, μ_{lb} were evaluated based on the local mean temperature of the fluid. Dynamic viscosity, μ_{lw}, was calculated based on the local wall inner surface temperature.

Relative discrepancy between the average heat transfer coefficients from experimental data and predicted values was found to be within 8.14%, and typical test data were presented in Fig. 6.

For the laminar flow of the pure water, the local heat transfer coefficients from experiments were compared with those calculated from Eq. (13), which was presented by Shah and London [27] and fitted well with the single-phase laminar developing flow in thermally developing region under a constant wall heat flux,

$$Nu_x = 5.364\left[1 + \left(\frac{220x^*}{\pi}\right)^{-10/9}\right]^{3/10} - 1.0$$

where

$$x^* = (x/D)/(Re_{\text{lb}} \cdot Pr_{\text{lb}}) \tag{13}$$

The comparison between the experiments values and predicted values calculated with Eq. (13) for a typical case is shown in Fig. 7. Relative discrepancy in average heat transfer coefficients between them was within 3.4%.

In the end portions of the measuring segment one can notice an increase in the measured local heat transfer coefficients in comparison to the values calculated according to Eqs. (12) and (13), which can be explained by the end region thermal effect of the test tube, because the temperature at the end of portions of measuring segments are higher than that at the beginning, so heat losses to the envi-

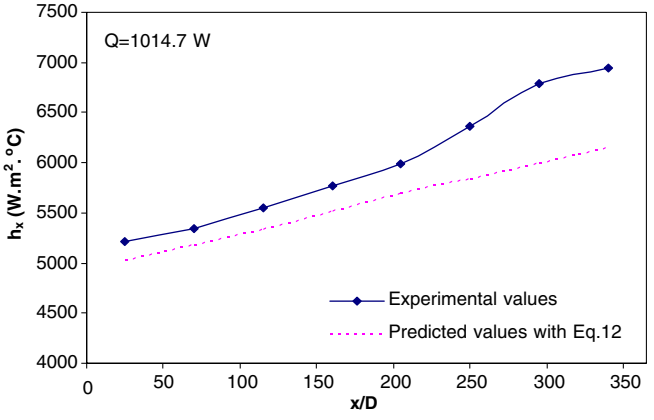

Fig. 6. Local heat transfer coefficients of pure water in turbulent condition ($Re_{\text{lb}} = 3475$–5073, $\dot{m} = 18.0$ g/s).

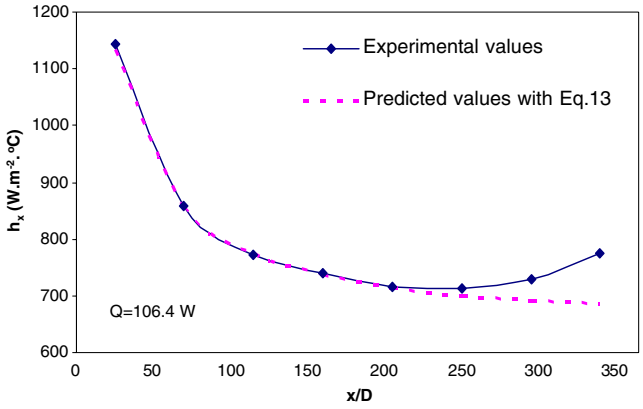

Fig. 7. Local heat transfer coefficients of pure water in laminar condition (Re_{lb} = 603–780, $\dot{m}$ = 2.96 g/s).

ronment of this section are also higher than the other sections.

It is concluded that the relative discrepancy between the measured values and values predicted using classical correlation equation both for the laminar flow and turbulent flow were small and within the acceptable range, taking into account the difficulty in controlling the experimental conditions and the universal applicability of the correlation equations. The local heat transfer coefficients for the slurry will be compared with the values calculated by Eqs. (12) and (13) in the subsequent discussions.

3.2.2. Laminar heat transfer characteristics of MPCM slurry

In Fig. 8, the evolution of the local Nusselt Number, Nu_x, is plotted against dimensionless axial distance, $x/(r_D RePr)$, particle mass concentrations of $w_p \sim 5\%$, 10% and 15.8% under the same heating rate across the test section, Q = 296.8 W, and mass flow rate, $\dot{m}$ = 4.95 g/s. The corresponding Nusselts numbers for pure water with the same heating rate calculated with Eq. (13) are also plotted in Fig. 8.

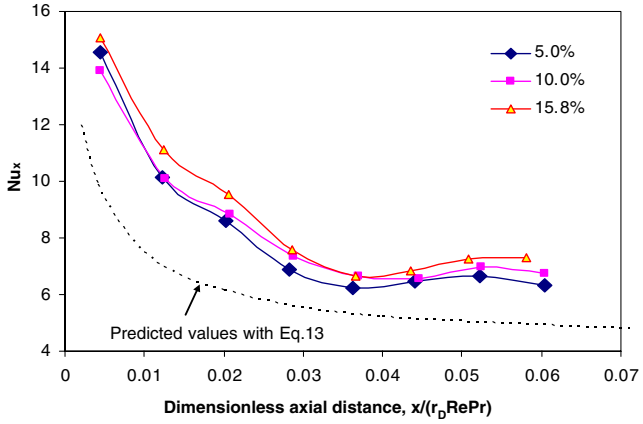

Fig. 8. Effects of particle mass concentration local Nusselt numbers.

As is shown in Fig. 8, the local Nusselt number in the thermally developing region are seen to increase by up to 56% when the mass particle fraction w_p = 15.8%. Such enhancement is attributed to melting latent heat effect of MPCS during phase change process, or the enhanced effective specific heat capacity of the slurry as proposed by Kasza and Chen [3], which is defined as

$$C_{p,eff} = C_p + w_p \Delta H_m / \Delta T \quad (14)$$

where w_p is the mass fraction of MPCM in the slurry; ΔH_m is the latent heat of the MPCM; ΔT is the difference between the slurry temperatures at the inlet and outlet of the test section. The latent heat of slurry increases with the mass faction, so does the effective specific heat capacity of the slurry. In Fig. 8, the local Nusselt numbers increased with mass particle fractions of the slurry, and they are all higher than the single-phase flow without phase change for all cases.

Fig. 9a and b show the calculated local bulk/mean temperatures, T_{lb}, and the corresponding local heat transfer coefficients, h_x, for pure water and MPCM slurry of w_p = 0.158 as well as the wall surface temperature operating with MPCM slurry. Bulk mean temperatures for slurry was calculated with the equations listed in Table 1. As is shown in Fig. 9a, the bulk temperature of pure water increased linearly along the flow direction. In the case of the MPCM slurry, the bulk temperature increased linearly along the test section in the Region I and Region III, while bulk temperature in the Region II kept at a constant value, T_{lb} = 14.3 °C, due to the latent heat release when PCM melted at nearly a constant temperature, T_m = 14.3 °C. In Fig. 9b, the calculated local heat transfer coefficients were higher than those of the pure water in the Region I and Region II, but approached those of the pure water in Region III. Such phenomena could be due to the following reasons: (1) the slurry temperatures near the tube wall were higher than the melting temperature of the PCM in Region

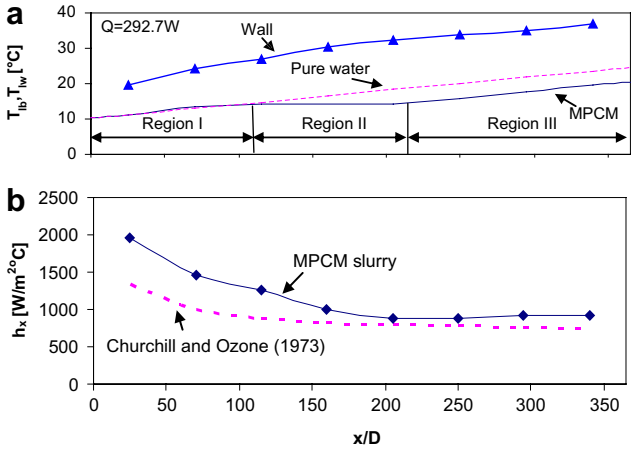

Fig. 9. (a) Local bulk mean temperatures, (b) local heat transfer coefficients for pure water and MPCM slurry of w_p = 0.158, Re_{lb} = 1196–1170 for pure water and Re_{lb} = 441–538 for slurry, at $\dot{m}$ = 4.95 g/s.

I, as shown in Fig. 9a, the internal wall surface temperature was almost higher than 20 °C, although the bulk mean temperatures are still lower than the melting temperature of the PCM, hence a small amount of PCM melted in the Region I, when more PCM particle melted, as a result, the enhanced heat transfer coefficients relative to pure water were found in Region I. (2) In the Region II, the bulk mean temperature was the same as that of melting temperature of PCM, PCM continued to melt and reached a maximum value, with the decreasing of melting PCM particles, the heat transfer coefficients was also decreasing gradually, and eventually approached those of the pure water at the end of this stage.

The local Nusselt Numbers are plotted against dimensionless axial distance in Fig. 10 for runs conducted at different Reynolds numbers and wall heat power inputs but at same particle mass fraction, $w_p = 0.158$.

Fig. 10 illustrates that the local Nusselt number are almost independent of heat power input and Reynolds number along the dimensionless axial distance of the test tube. Local Nusselt numbers for all cases are higher than those of the pure water. They also presented the similar trend along the axial distance as that of pure water in the thermal developing region at laminar flow velocities, and the local Nusselt number decreased along the flow direction at entry region, and then it approached the stable state when flow was fully developed. An interesting phenomenon is that all the experimental data points seem to form a consistent smooth curve. The similar results were also found for the slurry with slurry particle fractions of 0.1 and 0.05 which are presented in Appendix A. Based on the experimental data for different power inputs, flow conditions and slurry particle mass concentrations, a new correlation equation was proposed which is related to the Shah and Londons' model (in Eq. (13)) for laminar single-phase flows in the developing region under a constant heat flux, and is expressed by the following form:

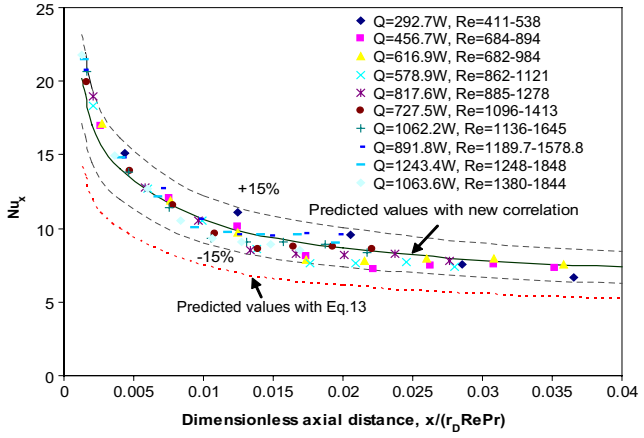

Fig. 10. Local Nusselt numbers vs. dimensional axial distance under different working conditions at $w_p = 0.158$.

Table 3
Values of c

Mass fraction (%)	c
5.0	1.336
10.0	1.341
15.8	1.418

$$\frac{Nu_{\text{MPCM slurry}}}{Nu_{\text{Shan and London}}} = c \tag{15}$$

where the values of c depends on the slurry particle fractions, which are presented in Table 3.

Fig. 10 compares the present experimental heat transfer results with those predicted with Eq. (15). All experimental data can be predicted by Eq. (15) within ±15%.

3.3. Turbulent heat transfer characteristics

Due to the increased viscosity associated with higher particle fractions, the heat transfer measurements were only performed for the slurry with particle concentrations of 5% and 10%. Fig. 11 shows the local heat transfer coefficients and the calculated bulk mean temperatures for MPCM slurry of $w_p = 5\%$ and pure water at the same mass flow rate and heating rate. The heat transfer coefficients of slurry were higher than those of pure water. Along the slurry flow direction, local heat transfer coefficient of water increased almost linearly, while heat transfer coefficient of slurry increased in Region I, decreased in Region II and increased again in Region III. Choi et al. [11] also reported the similar phenomenon occurred in the turbulent flow of phase change emulsion (mixture of water and PCM particles), and their explanations for this phenomenon is also suitable for present turbulent MPCM slurry flow, which are cited as follows: (1) In Region I, a small amount of MPCM melted near the wall because the

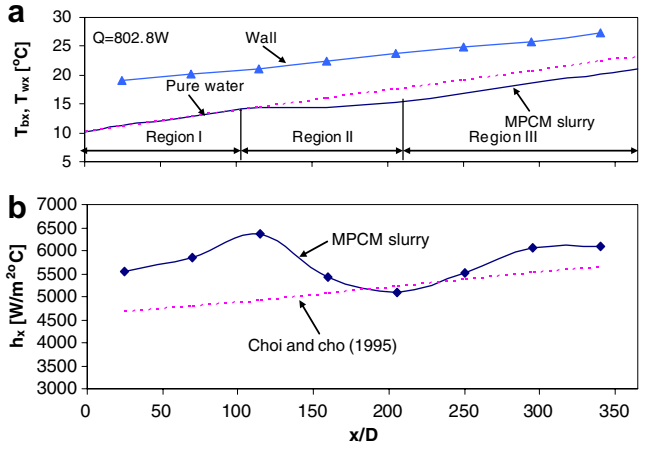

Fig. 11. (a) Local bulk mean temperatures, (b) local heat transfer coefficients for pure water and MPCM slurry of $w_p = 0.158$, $Re_{lb} = 3635–5015$ for pure water and $Re_{lb} = 2320–3068$ for slurry, at $\dot{m} = 16.4$ g/s.

wall temperature was higher than the melting temperature of 1-bromohexadecane (see Fig. 11a), although the bulk mean temperature was lower than the melting temperature due to the low temperature of slurry near the tube center line, therefore the heat transfer coefficient increased when more MPCM melted in Region I. (2) In Region II, the number of melted MPCM particles reached a maximum value when the bulk mean temperature of slurry reached the melting temperature of 1-bromohexedecane, and the heat transfer coefficient also reached a maximum value (point *m*). After that, the number of solid MPCM particle decreased gradually. In addition, the melted particles near the heated tube wall prevented the solid particles transporting to the wall, which in turn reduced the number of PCM particles involved in phase-change, so heat transfer coefficient decreased in Region II. (3) The local Reynolds number increased with the increased bulk mean temperature of slurry along the test section in Region III due to the rise of the slurry temperature, which resulted in the increased heat transfer coefficient in Region III.

Fig. 12 compares the heat transfer performance of MPCM slurry flow at two different heat rates, $Q = 802.8$ and 1139.3 W, and the mean flow velocity, the particle concentration and inlet temperature of slurry are the same for two cases. It is seen that the maximum value of heat transfer coefficient for higher heat rate appeared earlier than that for lower heating rate. Moreover, the heat transfer coefficient is higher than for higher heat rate after phase-change process. These might be due to the following reasons: (1) when the heating rate was higher, the length of Region I became shorter than that the lower heating rate case, which means the maximum value of MPCM particles involved in phase change began earlier, hence the maximum heat transfer coefficient appeared earlier, (2) when higher heating rate applied in the test tube, the temperature rise of the MPCM slurry was higher, the viscosity was lower than that for the case of lower heating rate in the Region III, thus the Reynolds number was also higher, therefore, the higher heat transfer coefficient was obtained for the high heating rate than that for the lower heating rate at the final stage of flow in the test tube.

In summary, the enhancement in heat transfer is accompanied with the undesirable increase of friction factor. There might exist an optimal concentration of PCM particles in the fluid considering the trade-off between the increased heat transfer and pressure loss as well as the effect on pump performance. For instance, Inaba et al. [30] presented their experimental results of heat transfer over the energy required to overcome the pressure loss, and found that a maximum exists at a particular PCM concentration. For a systematic optimization, the effect on pump performance would also be needed, and this will deserve separate study in future works.

The average Nusselt numbers are plotted in Fig. 13 for runs conducted at different Reynolds numbers and wall heat rates at particle fraction of 5% and 10% at Reynolds number $Re = 2100$–3452. The average Nusselt numbers from experiments presented were compared not only with predicted values with Eq. (12), but also with values with the correlation given by Gnielinski [28]. Gnielinski correlation equation can well predict the single-phase heat transfer coefficient in the Reynolds number range between 2300 and 10^4 under uniform heat flux conditions

$$Nu_{\mathrm{gn,m}} = \frac{(f/8)(Re_{\mathrm{D}} - 1000)Pr}{1 + 12.7(f/8)^{1/2}(Pr^{2/3} - 1)}$$

where

$$f = (1.82\log_{10}Re_{\mathrm{D}} - 1.64)^{-2} \tag{16}$$

As shown in Fig. 13, there are small differences between prediction values with Eqs. (12) and (15). The local Nusselt number increased with Reynolds numbers both for the slurry flow and pure water flow, the enhanced heat transfer performance was achieved for the slurry with particle frac-

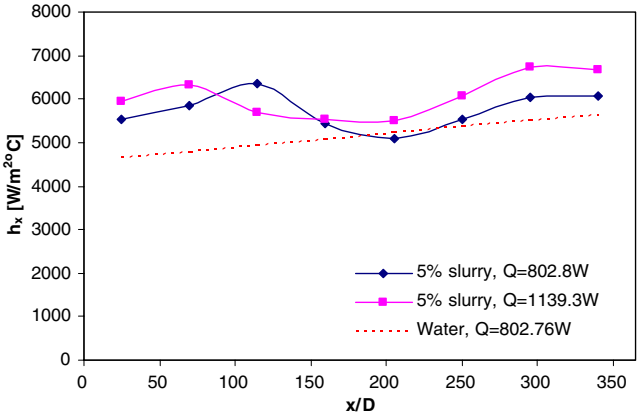

Fig. 12. Local heat transfer coefficients of MPCM slurry at different heating rates of 802.8 and 1139.3 W $Re_{\mathrm{lb}} = 3635$–5015 for pure water and $Re_{\mathrm{lb}} = 2320$–3503 for slurry, at $\dot{m} = 16.4$ g/s.

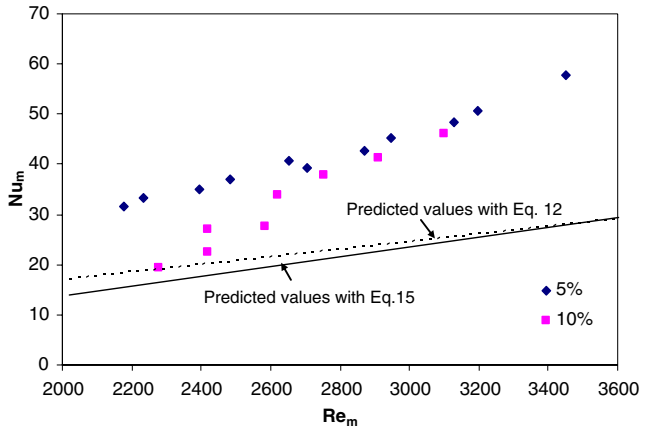

Fig. 13. Average Nusselt numbers of two different slurries with $w_{\mathrm{p}} = 0.05$ and 0.1 at Reynolds numbers $Re_{\mathrm{m}} = 2100$–3452.

tion of 5% and for the slurry with particle fraction of 10%, with 1–2.5 times higher average Nusselt numbers obtained in comparison with single-phase flow. A surprising result found in Fig. 13 is that the average Nusselt numbers for slurry of 5% particle faction were higher than those for 10% particle fraction at the same Reynolds number. Such phenomenon can be probably due to the degradation of the turbulent degree with higher loading of the particles with size of several microns. As reported by Liu et al. [29], there existed a threshold of particle size in augmentation of heat transfer when solid particles were added into a single-phase flow. When the particles are smaller than such sizes, a degradation of heat transfer will be achieved, and when particles are bigger than such sizes, there will be enhancement in heat transfer performance for a specific tube. Higher loadings of solid particles may further degrade the heat transfer performance. This is also the reason why heat transfer coefficient was lower than that of pure water just after all MPCM melted, as exhibited in Figs. 11b and 12.

4. Conclusions

The dynamic viscosity of slurries with particle mass concentration up to 27.6% were measured and fitted with the famous Vand's model, and all slurries in the present study exhibited Newtonian behaviors. The results of pressure drop measurements showed a distinct transition when slurry flow change from laminar to turbulent, and the friction factors in turbulent flow fitted well with the classical model based on Hagen–Poiseuille flow, while the friction factor in laminar flow were lower than those calculated from Blasius equation due to the entry length effect.

Experiments were performed in both laminar and slightly turbulent flow velocity ranges for MPCM slurry flowing in a horizontal circular tube with constant heating rates. The local heat transfer coefficients were measured and reported at steady state. The local heat transfer coefficients for MPCM slurry were higher than those for pure water due to the associated latent heat during phase-change process. In the case of laminar flow, the local heat transfer coefficients increased with the fraction of PCM particle in the fluid, and three distinct regions are found based on the calculated bulk mean temperature along the test section. In the case of turbulent flow, local heat transfer coefficients are significantly influenced by the heating rates across the test section, and the maximum values of heat transfer coefficient appeared earlier for a higher heating rate than for a lower heating rate. The average heat transfer coefficients as a function of mean Reynolds number are also calculated for the turbulent flow velocities, and were compared with those for single-phase fluid flow predicted by the correlation in the literature, it was found the heat transfer performance of MPCM slurry was quite influenced by the turbulent degree of the fluid.

A new laminar correlation equation was proposed from appropriate dimensionless group used in the conventional laminar convective correlations that could satisfactorily predict the local heat transfer data within the error of ±15%. The new correlation equation will be useful for the design of compact heat exchangers and thermal storage systems with MPCM slurry applications.

Acknowledgements

We are grateful to the Innovation Technology Commission and the Hong Kong Polytechnic University for providing support to this research through ITS-023-03, ITS-049-06 and A188.

Appendix A. Comparisons of experimental and predicted values of slurry $w_p = 5\%$ and 10% with new correlation

See Figs. A.1 and A.2.

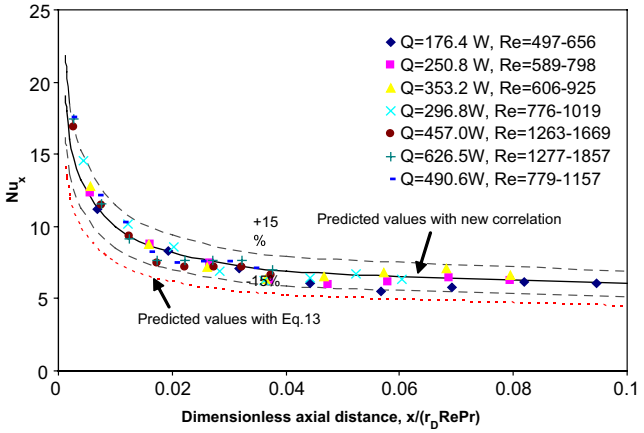

Fig. A.1. Comparison of experimental and predicted values of local Nusselt number with Eq. (15) of slurry $w_p = 5\%$.

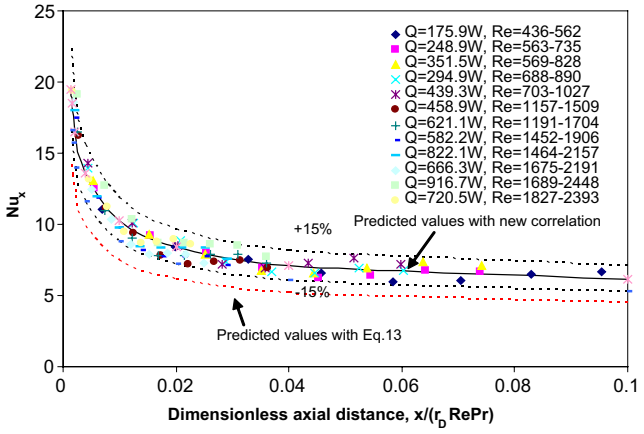

Fig. A.2. Comparison of experimental and predicted values of local Nusselt number with Eq. (15) of slurry $w_p = 10\%$.

References

[1] M.M. Farid, A.M. Khudhair, S.A.K. Razack, A.A. Hallaj, A review on phase change energy storage: materials and applications, Energy Convers. Manage. 45 (2004) 1597–1615.

[2] F. Wang, G. Maidment, J. Missenden, R. Tozer, A review of research concerning the use of PCMs in air conditioning and refrigeration engineering, Adv. Build. Technol. 2 (2002) 1273–1280.

[3] K.E. Kasza, M.M. Chen, Improvement of the performance of solar energy or waste heat utilization systems by using phase-change slurry as an enhancement heat-transfer storage fluid, J. Solar Energy Eng. 107 (1985) 229–236.

[4] C.W. Sohn, M.M. Chen, Microconvective thermal conductivity in disperse two-phase mixture as observed in a low velocity Couette flow experiment, J. Heat Transfer 103 (1981) 47–50.

[5] P. Charunyaorn, S. Sengupta, S.K. Roy, Forced convective heat transfer in microencapsulated phase change material slurries: flow in circular ducts, Int. J. Heat Mass Transfer 34 (3) (1991) 819–833.

[6] M. Goel, S.K. Roy, S. Sengupta, Laminar forced convection heat transfer in microencapsulated phase change material suspensions, Int. J. Heat Mass Transfer 37 (4) (1994) 593–604.

[7] Y. Zhang, A. Faghri, Analysis of forced convection heat transfer in microencapsulated phase change material suspensions, J. Thermophys. Heat Transfer 9 (4) (1995) 727–732.

[8] E.L. Alisetti, S.K. Roy, Forced convection heat transfer to phase change materials slurries in circular ducts, J. Thermophys. 14 (1) (1999) 115–118.

[9] X. Hu, Y. Zhang, Novel insight and numerical analysis of convective heat transfer enhancement with microencapsulated phase change material slurries: laminar flow in a circular tube with constant heat flux, Int. J. Heat Mass Transfer 45 (2002) 3163–3172.

[10] C.J. Ho, J.F. Lin, S.Y. Chiu, Heat transfer of solid–liquid phase-change material suspensions in circular pipes: effects of wall conduction, Numer. Heat Transfer: Part A 45 (2004) 171–190.

[11] E. Choi, Y. Cho, H.G. Lorsch, Forced convection heat transfer with phase-change-material slurries: turbulent flow in a circular tube, Int. J. Heat Mass Transfer 37 (2) (1993) 207–215.

[12] Y. Yamagishi, H. Takeuchi, A.T. Pyatenko, Characteristics of microencapsulated PCM slurry as a heat-transfer fluid, AIChE J. 45 (4) (1999) 696–707.

[13] E.C. Guyer, D.L. Brownnell, Handbook of Applied Thermal Design, McGraw-Hill, New York, 1988.

[14] D.J. Jeffrey, Conduction through a random suspension of spheres, Proc. R. Soc. Lond. A (1973) 335–367.

[15] L.G. Leak, On the effective conductivity of a dilute suspension of spherical drops in the limit of flow particle Peclet number, Chem. Eng. Commun. 1 (1973) 21–31.

[16] J.C. Maxell, A Treatise on Electricity and Magnetism (third ed.), vol. 1, Dover, New York, 1954, pp. 440–441.

[17] R. Holmen, M. Lamvik, O. Melhus, Measurements of thermal conductivities of solid and liquid unbranched alkanes in the C16-to-C19 range during phase, Int. J. Thermophys. 23 (1) (2002) 27–39.

[18] Yaws, L. Carl, Yaws' Handbook Thermodynamic and Physical Properties of Chemical Compounds, Knovel, Norwich, New York, 2003.

[19] J.A. Dean, Lange's Handbook of Chemistry, 15th ed., McGraw-Hill, New York, 1999.

[20] A. Bejan, A.D. Kraus, Heat Transfer Handbook, John Wiley & Sons, Inc., Hoboken, NJ, 2004.

[21] V. Ayel, O. Lottin, H. Peerhossaini, Rheology, flow behavior and heat transfer of ice slurries: a review of the state of the art, Int. J. Refrig. 26 (2003) 95–107.

[22] R.W. Allen, E.R.G. Eckert, Friction and heat-transfer measurements to turbulent pipe flow of water ($Pr = 7$ and 8) at uniform wall heat flux, J. Heat Transfer 86 (1964) 301–310.

[23] V. Vand, Theory of viscosity of concentrated suspensions, Nature 155 (1945) 364–365.

[24] J.C. Mulligan, D.P. Colvin, Y.G. Bryan, Microencapsulated phase-change material suspensions for heat transfer in spacecraft thermal systems, J. Spacecraft Rackets 33 (2) (1996) 278–284.

[25] F.P. Incropera, D.P. Dewitt, Introduction to Heat Transfer, third ed., John Wiley & Sons, Inc., 1996, pp. 392–393.

[26] E. Choi, Y.I. Cho, Local friction and heat transfer behavior of water in a turbulent pipe flow with large heat flux at the wall, J. Heat Transfer 117 (1995) 283–288.

[27] R.K. Shah, A.L. London, Laminar Flow Forced Convection in Ducts, Academic Press, New York, 1978, pp. 128–129.

[28] W.M. Kays, M.E. Crawford, B. Weigand, Convective Heat and Mass Transfer, McGraw-Hill, New York, 2005, pp. 297–299.

[29] K.V. Liu, U.S. Choi, K.E. Kasza, Pressure drop and heat transfer characteristics of nearly buoyant particulate slurry for advanced energy transmission fluids, Int. Symp. Liquid–Solid Flows (1988) 107–113.

[30] H. Inaba, M.J. Kim, A. Horibe, Melting heat transfer characteristics of microencapsulated phase change material slurries with plural microencapsules having different diameters, Trans. ASME 126 (4) (2004) 558–565.